DEVELOPMENT AND VALIDATION OF A ROBUST CFD PROCEDURE FOR PREDICTING INDOOR ROOM AIR MOTION

A.J. Baker[1], P.T. Williams[1], and R.M. Kelso[2]

[1] Department of Engineering Science and Mechanics, University of Tennessee, Knoxville, TN, USA
[2] School of Architecture, University of Tennessee, Knoxville, TN, USA

ABSTRACT

The requirement is attainment of high quality computational (CFD) solutions to the Reynolds-averaged Navier-Stokes equations for buoyant and turbulent flows in three-dimensional indoor geometries. Popular CFD theory/codes stabilize intrinsic dispersive error via artificial diffusion methods, with resultant compromise of genuine physical diffusion processes. A new Taylor weak statement CFD theory, and finite element code implementation, represents a potential significant accuracy/stability improvement for 3-dimensional buoyant room air flow prediction. This theory and documentary validations are summarized in this paper.

INTRODUCTION

Computational fluid dynamics (CFD) is the maturing art/science of computer-generation of approximate solutions to the Reynolds-averaged Navier-Stokes (RaNS) equations. A CFD algorithm can (*at best!*) generate only an *approximate solution*, and intrinsic dispersive error mechanisms exist to compromise stability, hence accuracy. Further, in room air motion simulation, the "CFD pressure" functions kinematically in enforcing mass conservation, and subtle pressure differential errors can have profound impact on flow directionality. These issues require very specific CFD modeling, whence *any* CFD algorithm transforms the selected non-linear RaNS partial differential equation (PDE) system into a much larger algebraic system amenable to "*computing*."

The Taylor weak statement (TWS) theory [1] with current generalizations [2], is proving capable of recovering most historical CFD dissipative methods for dispersion error control. This paper highlights this TWS theory, applied to RaNS, and its semi-discretization via a finite element implementation of a Galerkin weak statement. Theoretical and computational performance validations are summarized for select 2-D benchmark and 3-D room air motion problem specifications.

THE PROBLEM STATEMENT

A statistical manipulation yields the RaNS PDE system governing thermal room air flows. Following nondimensionalization, and identifying the turbulent

Reynolds number (Re^t) of the turbulence closure model, the governing basic PDE system for solution is

$$\mathcal{L}(u_i) = \frac{\partial u_i}{\partial t} + \frac{\partial}{\partial x_j}\left(u_i u_j + P\delta_{ij} - \frac{1}{Re}\left(1 + Re^t\right)\left(\frac{\partial u_i}{\partial x_j} + \frac{\partial u_j}{\partial x_i}\right)\right) - Ar\Theta\delta_{ig} = 0 \qquad (1)$$

$$\mathcal{L}(\Theta) = \frac{\partial \Theta}{\partial t} + \frac{\partial}{\partial x_j}\left(u_j\Theta - \frac{1}{Re}\left(\frac{1}{Pr} + \frac{Re^t}{Pr^t}\right)\frac{\partial \Theta}{\partial x_j}\right) - s_\Theta = 0 \qquad (2)$$

along with the continuity constraint of divergence-free mean-flow velocity vector $u_i(x_j, t)$. Additional definitions in (1)-(2) include potential temperature, $\Theta \equiv (T - T_{min})/(T_{max}-T_{min})$, and kinematic pressure $P = p/\rho_0 + 2k/3$, where k is turbulence kinetic energy. The dimensionless groups are Reynolds number (Re), Archimedes number ($Ar=Gr/Re^2$), hence the Grashoff number (Gr), and Prandtl number (Pr). A superscript "t" denotes the modeled "turbulent" counterpart.

The character of solutions to (1)-(2) depends on these groups, the distribution of Re^t and boundary conditions. Since Re>0 and $Re^t \geq 0$, each isolated equation is elliptic, hence the mean-flow state variable $q\,(x, t) = \{u_1, u_2, u_3, \Theta\}^T$, and/or its normal derivative, is required known all around the problem statement boundary. The solution process is thus classic initial-boundary value, up to enforcement of the continuity constraint that u_i is divergence-free. This differential constraint becomes enforced kinematically, via *inexact* CFD theories, as a modelled action of pressure P. One construction appends a Poisson equation

$$\mathcal{L}(\phi) \equiv -\nabla^2\phi - \nabla\cdot\tilde{\mathbf{u}}_{n+1} = 0 \qquad (3)$$

to (1)-(2), where superscript tilde denotes *any* approximation to the true velocity $\mathbf{u}$, and n is the time-step index. The solution ϕ is then manipulated into a pressure approximation $P^{n+1}_A \cong P^n - \phi_{n+1}/\theta\Delta t$, which may then selectively be replaced via the genuine pressure, a solution to

$$\mathcal{L}(P) = \frac{\partial^2 P}{\partial x_i^2} + \frac{\partial}{\partial t}\left(\frac{\partial u_i}{\partial x_i}\right) + \frac{\partial^2}{\partial x_i x_j}\left(u_i u_j - \frac{1}{Re}\left(1 + Re^t\right)\left(\frac{\partial u_i}{\partial x_j} + \frac{\partial u_j}{\partial x_i}\right)\right) - Ar\frac{\partial \Theta}{\partial x_g} = 0 \qquad (4)$$

Appropriate boundary conditions are required to render (3)-(4) well-posed, cf., Baker, et.al. [3]. Finally, a closure model to determine Re^t is required.

WEAK STATEMENT CFD ALGORITHM

A CFD algorithm for (1)-(4) generates solutions characterized by Re, Gr, Pr and Re^t, since $Pr^t \approx Pr$. The CFD state variable is $q(x_j, t) = \{u_1, u_2, u_3, \Theta; \phi, P\}^T$, which by partition (at the semi-colon) satisfies the PDE systems

$$\mathcal{L}(q) = \frac{\partial q}{\partial t} + \frac{\partial}{\partial x_j}\left(f_j - f_j^v\right) - s = 0 \qquad (5), \qquad \mathcal{L}(q_a) = \nabla^2 q_a - s(q) = 0 \qquad (6)$$

In (5), $f_j = f_j(q)$ is the kinematic flux vector while f_j^v is the dissipation flux-vector embodiment of the turbulence closure model plus natural diffusion. In (6), the laplacian operates on $q_a = \{\phi, P\}^T$, and $s = s(q)$ are the respective source term.

Any CFD algorithm generates an approximation to the true solution to (5)-(6) via a denumerable set of decisions leading to an algebraic system amenable "to computing." A dominating dispersive error mechanism is intrinsic to this process for (5), ultimately leading to use of "artificial diffusion" mechanisms, e.g., "QUICK" differencing. The Taylor weak statement theory [1]-[2], extended to systems (5) yields creation of the PDE companion to (5) as

$$\mathcal{L}^c(q) \equiv \mathcal{L}(q) - \beta\Delta t\frac{\partial}{\partial x_j}\left(A_j A_k \frac{\partial q}{\partial x_k}\right) \qquad (7)$$

where $A_j \equiv \partial f_j/\partial q$ is the kinematic flux vector jacobian. Thereafter, any approximation $q^N(\mathbf{x}, t)$ to the true solution to (6) - (7) in the continuum is

$$q(x, t) \approx q^N(x, t) \equiv \sum_{j=1}^{N} \Psi_j(x)\, Q_j(t) \qquad (8)$$

where $\Psi_j(x)$ are assumed known functions and $Q_j(t)$ are the associated time-dependent unknown expansion coefficients. Since q^N cannot satisfy (6)-(7), the error associated with q^N is minimized by requiring the Taylor weak statement

$$TWS = \int_\Omega \Phi_i(x)\,\mathcal{L}^c(q^N)\, d\tau = 0\,, \quad \forall i \qquad (9)$$

be satisfied for any (all) known functions $\Phi_i(x)$. If the theory-designer picks $\Phi_i(x)$ and $\Psi_i(x)$ identical, a "Galerkin finite element" (FE) statement results. Conversely, if one chooses $\Phi_i(x)$ to be constants, then a "finite volume" (FV) form is produced. Thereupon, the pertinent spatial semi-discretization permits evaluation of the integrals defined in TWS, which for (7) always produces a matrix ordinary differential equation (ODE) system of the form [4]

$$TWS^h = [M]\frac{d\{Q\}}{dt} + \{R(Q)\} = \{0\} \qquad (10)$$

where superscript h denotes "discretization," $[M]$ and $\{R\}$ are global rank square and column matrices, and $\{Q\} = \{Q(t)\}$ is the state variable approximation coefficient set at the nodes of the mesh Ω^h. Any ODE algorithm uses (10) for time derivative evaluation; selecting the one-step θ implicit procedure, for example, produces the terminal algebraic matrix equation for computing as

$$\{FQ\} = [M]\{Q_{n+1} - Q_n\} + \Delta t\left(\theta\{R\}_{n+1} + (1-\theta)\{R\}_n\right) = \{0\} \qquad (11)$$

where "n" denotes time step level. The discrete Galerkin weak statement for the Poisson equation (6) directly produces the matrix system

$$\{FQ_A\} = [D]\{Q_A\} - \{S(Q)\} = \{0\} \qquad (12)$$

where square matrix $[D]$ is the discrete laplacian, $\{Q_A\}$ is the nodal array of ϕ^h or P^h, and $\{S(Q)\}$ contains dependence on q^h via solution $\{Q(t)\}$ from (11).

The generic solution process for (11)-(12) is a numerical linear approximation to the Newton iteration algorithm

$$[J]\{\delta Q\}_{n+1}^{p+1} = -\{F\}_{n+1}^{p} \qquad (13), \qquad \{Q\}_{n+1}^{p+1} = \{Q\}_n + \sum_{i=0}^{p} \{\delta Q\}_{n+1}^{i+1} \qquad (14)$$

where $[J]$ is the "jacobian" of (11)-(12). The Newton jacobian in (13) is formed using calculus operations; thereafter, the range of quasi-Newton iterative procedures use approximations in concert with iterative cyclings, e.g., Gauss-Seidel, GMRES, preconditioned conjugate gradient, etc.

ACCURACY, STABILITY AND DISPERSION

The fundamental CFD decision is selection of the trial and test spaces, in defining q^N and the TWS error constraint respectively. In the semi-discrete implementation, this is commensurate with algorithm order of accuracy, hence asymptotic convergence under mesh refinement. Linear FE and traditional FV algorithms are typically second-order accurate, c.f., [4, Ch. 4, 6].

Algorithm stability is of greater practical significance, as related principally to control of the third-order dispersive error mechanism. Specifically, any mesh of measure $h = \Delta x$ is incapable of resolving information of wavelength $2\Delta x$, yielding the characteristic, cascading $2\Delta x$ oscillatory dispersive error mode. The non-linearity of the NS equation system amplifies this dispersion error, which is typically damped numerically to produce convergent iteration hence smooth solution. Figure 1 summarizes recent [2] phase velocity and amplification factor determinations for several popular FV algorithms, and GWS^h and TWS^h linear (GL) and quadratic (GQ) FE basis algorithms. The performance of the FE forms is clearly superior.

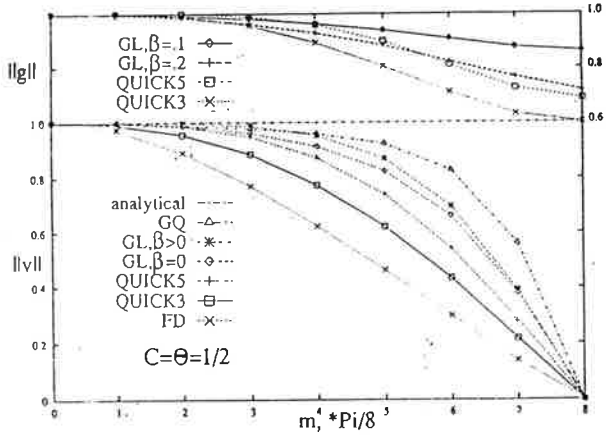

Figure 1. Fourier amplification factor ||g|| and phase velocity ||v|| for various CFD algorithms.

DISCUSSION AND RESULTS

The benchmark problem of specific pertinence to room air motion is the close-coupled step wall diffuser, cf., [5], which models the essence of a supply outlet. Figure 2 summarizes the 2-D Galerkin WS^h steady state laminar solution obtained at Re = 389 in terms of velocity vector $\mathbf{u}^h$ distribution (a), with experimental location of separation zone reattachment (x_1/S) noted, and pressure (b). In proceeding to Re = 648, a secondary separation occurs (c), in qualitative agreement with experiment (in 3-D), however, the pressure field (d) is quite polluted by a dispersive error mode in $\mathbf{u}^h$. Switching to the TWS^h dissipative algorithm, with β=0.1, does not measurably alter $\mathbf{u}^h$ but totally annihilates the pressure oscillations (e). Similar trends are recorded for the fully 3-D benchmark simulation, to be reported elsewhere.

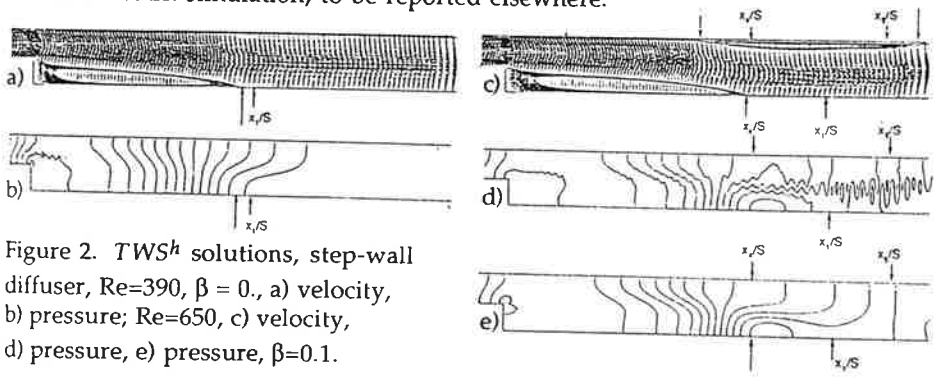

Figure 2. TWS^h solutions, step-wall diffuser, Re=390, β = 0., a) velocity, b) pressure; Re=650, c) velocity, d) pressure, e) pressure, β=0.1.

The pertinent 3-D thermal room air CFD experiment is for the partitioned-room geometry of Neymark [6]. Figure 3(a) illustrates the essential configuration, constituted of opposed heated and cooled walls with chamber partition containing a doorway of adjustable aspect ratio. The water experiments (Pr=6) remained laminar for $10^6 \le GrPr = Ra \le 10^9$, and confirmed a natural convection-induced jet enters the colder room vertically at the door jamb. The symmetric domain non-uniform mesh contains ~57,000 nodes; Fig. 3(b) is a cut-away view. Fig. 3(c) presents the steady-state $\mathbf{u}^h$ field at Ra=10^6, β=0.1, on select nodal planes.

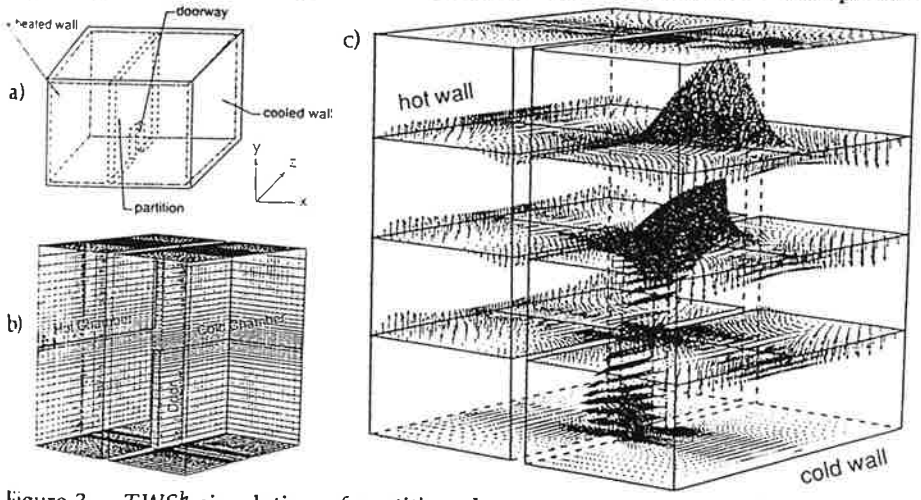

Figure 3. TWS^h simulation of partitioned-room geometry of [6], a) sketch of problem, b) FE mesh, c) steady-state velocity field, Ra = 10^6, β = 0.1.

Figures 4(a)-(d) summarize companion isotherm distributions on select vertical planes, along with associated $\mathbf{u}^h$ distributions. These results are in good qualitative agreement with experimental data; page limitations preclude a more detailed discussion here.

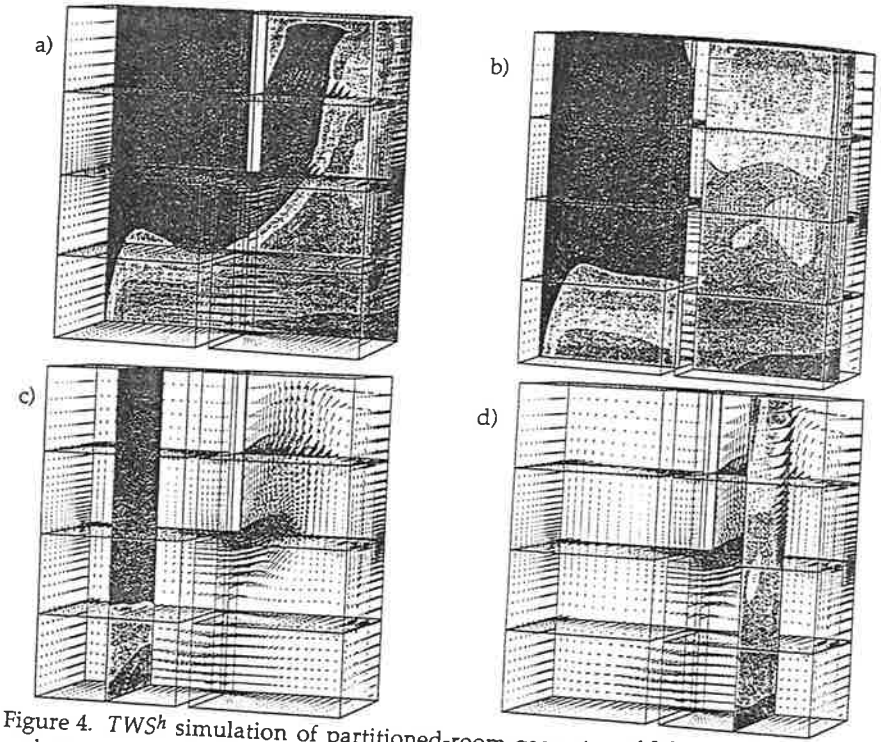

Figure 4. TWS^h simulation of partitioned-room geometry of [6], Ra=10^6, velocity and temperature distributions on symmetry- (a) and select (b-d) quarter-planes.

SUMMARY AND CONCLUSIONS

A FE spatial semi-discretization of a Taylor weak statement forms the theoretical basis for a new CFD algorithm, for application to prediction of thermal room air motion. The formulation ingredient of stability, without excess artificial diffusion, is validated for a benchmark. A three-dimensional solution is discussed for a natural convection, two-partition room geometry.

ACKNOWLEDGMENTS

This research is partially supported by NSF under Grant MSS-9015912 which is gratefully acknowledged, as are the corporate sponsors of the UT CFD Laboratory.

REFERENCES

1. Baker, A. J. and Kim, J. W., Int. J. Num. Mtd. Fluids, V.7, pp. 489-520, 1987.
2. Chaffin, D. J., private communication, 1993
3. Baker, A. J., P. T. Williams, R. M. Kelso, ASHRAE Trans, 1993, to appear.
4. Baker, A. J., Hemisphere Publishing, Washington, D.C., 1983.
5. Armaly, B. F., et. al., J. Flu. Mech. V. 127, pp. 473-496, 1983.
6. Neymark, J., M.Sc. Thesis, Colo. State Univ., 1988.

AIR FLOW PATTERN AND POLLUTANT TRANSMISSION IN AUDITORIA - MEASUREMENTS AND CFD-SIMULATIONS

Finn Drangsholt

SINTEF applied thermodynamics, NTH, Trondheim, Norway

ABSTRACT

This paper deals with air flow pattern and pollutant transmission in auditoria. Through different tracer gas techniques the air distribution and the removal of contaminants inside auditoria have been classified in terms of air exchange efficiency, local air change index, ventilation effectiveness and local ventilation index. Situations with various occupancy and ventilation rate have been studied.

The tracer gas measurements were supplemented and generalized by numerical simulations carried out with the CFD code KAMELEON. The simulations have shown that the air flow pattern inside this type of premises may be quite complex. The air flow pattern is affected by room geometry, capacity and location of heat source, aspects of building materials and construction, furnishing, the ventilation principle, supply air temperature and surrounding climate.

A general trend from simulations of terraced premises is that the upper part of the occupied zone appears to be the most polluted area with regard to both thermal and atmospherical contaminants. This tendency is independent of the ventilation principle and technical layout.

INTRODUCTION

The air flow pattern within a zone can have a considerable impact on the indoor air quality, the thermal comfort and the energy performance of the ventilation system. Studies in auditoria, carried out by the author, have shown that the air flow pattern and the pollutant transmission are affected by many parameters. These include room geometry, capacity and location of heat source, building fabrics, furnishing, ventilation principle, leakages and short circuiting, supply air temperature and surrounding climate.

Even with a sophisticated measuring concept, it is difficult to consider in detail the pattern of the air flow, or the influence from air movement on thermal and pollutant transport. Computational fluid dynamics (CFD) enables the air flow pattern to be predicted within a zone with a wealth of details, if sufficient computer resources are available.

The objective of this work has been to verify and visualize the impact of parameters affecting the air flow pattern inside auditoria with terraced floor. The work was accomplished by carrying out full scale measurements and CFD computations of the air flow pattern and pollutant transmission.